

Axial Transient Vibration of Polygonal Mirror Scanner Motor Supported by Thrust Magnetic Bearing and Radial Air Bearing

Hiroyuki Kawamoto^{▲*}

Corporate Research Laboratories, Fuji Xerox Co., Ltd., Kanagawa, Japan

This article describes an axial transient vibration of a polygonal mirror scanner rotor driven by a flat-type brushless DC motor and supported by a passive thrust magnetic bearing and a radial air bearing. From results of theoretical and experimental investigations, the following characteristics of the vibration, countermeasures to suppress a static displacement, and the transient vibration have been deduced: (1) Repulsive magnetic force is induced between the stator coils and rotor magnet under current passage. The force is proportional to the motor current. The force causes axial static displacement and axial transient vibration. (2) Parametric investigation deduced that: (a) higher stiffness of the magnetic bearing and lower acceleration current linearly reduce both the static displacement and the transient vibration; however, the former may reduce lifetime of the air bearing due to a dry contact with start and stop operation, and the latter prolongs the startup time; (b) soft start-stop scheme of the motor current is effective to reduce the vibration.

Journal of Imaging Science and Technology 43: 484–491 (1999)

Introduction

A polygonal mirror scanner motor is used in the exposure subsystem of digital xerography to scan the laser beam and to write latent images on the photoreceptor.^{1,2} The rotation of the mirror is required to be

- (1) stable, constant velocity, and low vibration, to realize high image quality,
- (2) high speed rotation for high print speed and high resolution machines,
- (3) long life,
- (4) small heat loss,
- (5) low acoustic noise, and
- (6) low cost.

The motor shown in Fig. 1 and Fig. 2 is under development to meet these requirements. The rotor is driven by a flat-type brushless and coreless DC motor. The polygonal mirror is attached to the rotor. The rotor is supported in the radial direction by an outer-rotor-type self-acting grooved journal air bearing^{3–6} and in the axial direction by an axially stable type passive magnetic bearing.^{7,8} The magnetic bearing utilizes an axial restoring magnetic force between a radially magnetized rotor magnet and a steel substrate of an electronic circuit board. Large axial transient vibration sometimes takes place in this rotor system during the startup operation. This prolongs the startup time, and in the worst case the rotor collides with a casing.

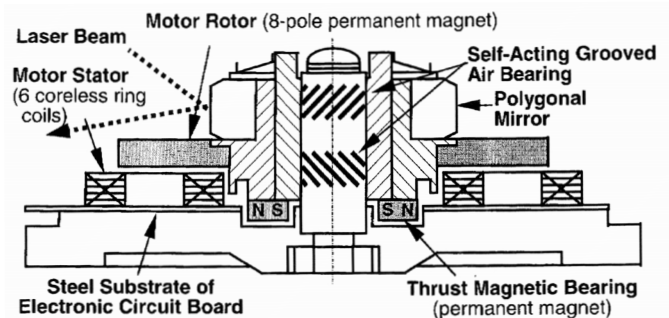


Figure 1. Configuration of polygonal mirror scanner rotor driven by flat-type brushless DC motor and supported by thrust magnetic bearing and radial air bearing.

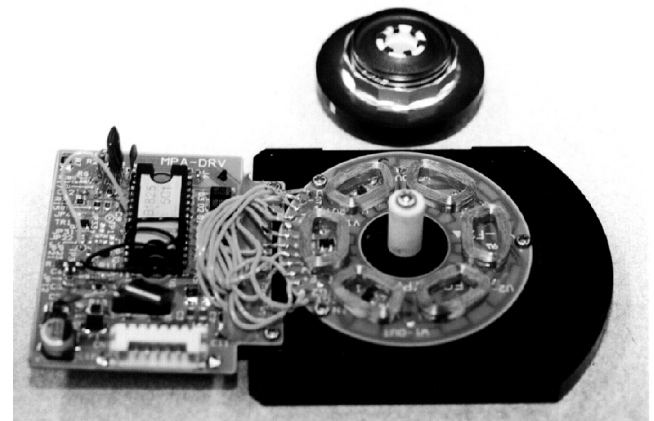


Figure 2. Polygonal mirror scanner motor. The rotor (upper) is disassembled from the stator (lower).

Original manuscript received November 11, 1998

▲ IS&T Member

* Current address: Department of Mechanical Engineering, Waseda University, Tokyo, Japan

© 1999, IS&T—The Society for Imaging Science and Technology

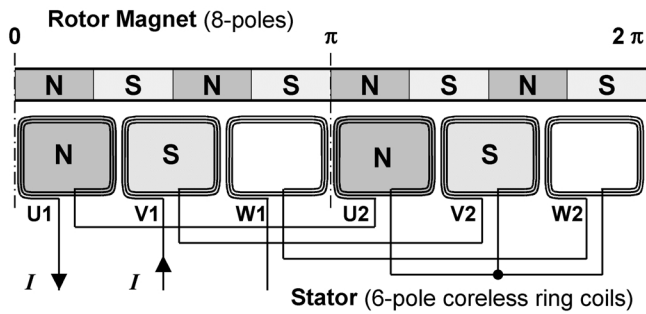


Figure 3. Development of motor rotor and stator. Upper: developed ring shape rotor (8-pole permanent magnet), lower: motor stator (3-phase 6-pole coreless ring coils)

Tada, Yanabe and Inoue⁹ reported characteristics of axial vibration of an optical disc-spindle-bearing system that was driven by the flat-type DC motor and supported by ball bearings. They concluded that the vibration was induced by the axial magnetic force due to an irregularity of the six stator coils of the driving motor. However, this mechanism cannot be applied to the present issue, because the vibration of the optical disc-spindle-bearing system was not transient but steady and the magnitude of vibration was in the order of micrometers which was more than one hundredth times smaller than that of our scanner motor. Ono and co-workers⁵ reported analysis and design of the radial air bearing and the thrust magnetic bearing for the polygonal scanner rotor-bearing system. The bearing system is similar to the present case. However, the axial transient vibration was not mentioned in the report because the motor is not the flat-type but a popular cylindrical type that does not induce the axial force.

The objectives of the present investigation are to clarify a mechanism of the large axial transient vibration observed in the rotor system driven by the flat-type DC motor and supported by the thrust magnetic bearing and the radial air bearing and to propose effective counter measures against its cause in order to realize highly reliable digital copy machines and laser printers.

Mechanism of Axial Transient Vibration

Figure 3 shows the development of the DC motor and Fig. 4 is a timing chart of current. The motor consists of a ring-shape rotor made of 8-pole permanent magnet and six coreless stator coils. The stator coils, which consist of three pairs of U, V, and W-phase coils, are star-connected as shown in Fig. 4. When the rotor is located at the position shown in Fig. 3, the current I flows from V-phase to U-phase. Circumferential force is induced in the radial sides of the coils based on the Fleming's rule and the rotor is accelerated. At the same time, the upper sides of V-phase and U-phase coils become N-pole and S-pole, respectively. The axial force between the V-phase coils and the rotor magnet is canceled, because the V-phase coils are located in the middle of the N-pole and the S-pole of the permanent magnet. On the other hand, the axial repulsive force is induced between the U-phase coils and the rotor magnet. Therefore, the total axial force is repulsive and its magnitude is proportional to the current. The axial transient forced vibration is induced at the start and stop of operation when the lumped axial force is induced. This hypothesis of the

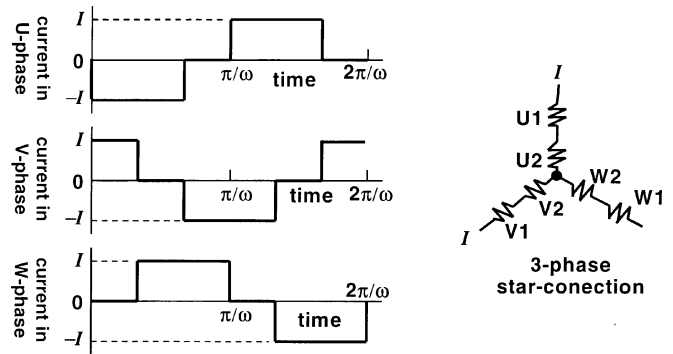


Figure 4. Timing chart of motor current in 3-phase star-connected stator coils.

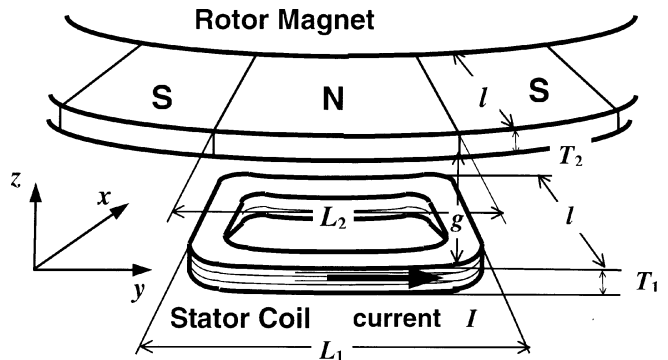


Figure 5. Single rotor magnet and stator coil.

axial transient vibration mechanism is confirmed analytically and experimentally in the following sections.

Modeling

Axial Magnetic Force Induced in Flat-Type DC Motor. First, the axial magnetic force induced in the flat-type DC motor is estimated. The configuration of single coil and single pole of the permanent magnet, shown in Fig. 5, is simplified as the rectangular two-dimensional model shown in Fig. 6.⁸ Here, L_1 and T_1 are the width and the thickness of the coil, L_2 and T_2 are the width and the thickness of the single pole of the permanent magnet, z_0 is the motor gap, y_0 is the circumferential lag between the rotor and the stator, and l is the width in the x -direction. The magnetic property of permanent magnet is assumed to be isotropic and its magnetic permeability is equal to that of the free space μ_0 . I' is an equivalent current corresponding to the coercive force H' of the permanent magnet. The winding thickness of the coil is assumed to be zero. The magnetic effect of the steel substrate is also neglected, i.e., the permeability of the system is assumed to be uniform.

The force f per unit length in the x -direction is the summation of the repulsive forces between the surfaces A and A' and between B and B' plus the attractive forces between A and B' and between B and A'.

$$f = -f_{AA'} - f_{BB'} + f_{AB'} + f_{BA'} \cong f_x \mathbf{i} + f_y \mathbf{j} + f_z \mathbf{k}, \quad (1)$$

where $(\mathbf{i}, \mathbf{j}, \mathbf{k})$ are the unit vectors in the (x, y, z) directions, respectively. The force $f_{AA'}$ is derived by the Biot-Savart law.

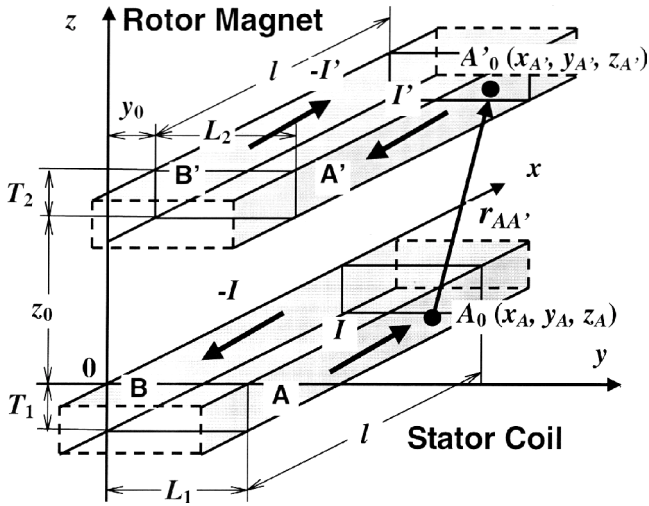


Figure 6. Two-dimensional simplified model to calculate repulsive magnetic force between a pair of permanent magnet and stator coil.

$$f_{AA'} = \lim_{l \rightarrow \infty} \frac{\mu_0 H H'}{2\pi l} \int_{z_0}^{z_0+T_0} \int_{-T_1}^0 \int_0^l \int_0^l \frac{\mathbf{r}_{AA'}}{r_{AA'}^3} dx_A dx_{A'} dz_A dz_{A'}, \quad (2)$$

where $\mathbf{r}_{AA'}$ is a distance vector from a point $A_0(x_A, y_A, z_A)$ on the surface A and a point $A'_0(x_{A'}, y_{A'}, z_{A'})$ on the surface A', and $r_{AA'}$ is its absolute value. H is the magnetomotive force of the coil. The distance vector $\mathbf{r}_{AA'}$ is expressed in the analytical form and the analytical integration of Eq. 2 is possible. The other forces $f_{BB'}$, $f_{AB'}$, $f_{BA'}$ are also calculated with the same procedure. The following is a derived analytical expression of the axial force.

$$\begin{aligned} f_z = & \frac{\mu_0 H H'}{4\pi l} \left\{ z_0 \log \frac{(z_0^2 + y_0^2)^2}{\left[z_0^2 + (y_0 - L_1)^2 \right] \left[z_0^2 + (y_0 + L_1)^2 \right]} \right. \\ & - (z_0 + T_1) \log \frac{\left[(z_0 + T_1)^2 + y_0^2 \right]^2}{\left[(z_0 + T_1)^2 + (y_0 - L_1)^2 \right] \left[(z_0 + T_1)^2 + (y_0 + L_2)^2 \right]} \\ & - (z_0 + T_2) \log \frac{\left[(z_0 + T_2)^2 + y_0^2 \right]^2}{\left[(z_0 + T_2)^2 + (y_0 - L_1)^2 \right] \left[(z_0 + T_2)^2 + (y_0 + L_2)^2 \right]} \\ & - (z_0 + T_1 + T_2) \log \frac{\left[(z_0 + T_1 + T_2)^2 + y_0^2 \right]^2}{\left[(z_0 + T_1 + T_2)^2 + (y_0 - L_1)^2 \right] \left[(z_0 + T_1 + T_2)^2 + (y_0 + L_2)^2 \right]} \\ & + 4y_0 \left[\tan^{-1} \frac{z_0}{y_0} - \tan^{-1} \frac{z_0 + T_1}{y_0} - \tan^{-1} \frac{z_0 + T_2}{y_0} + \tan^{-1} \frac{z_0 + T_1 + T_2}{y_0} \right] \\ & - 2(y_0 + L_2) \left[\tan^{-1} \frac{z_0}{y_0 + L_2} - \tan^{-1} \frac{z_0 + T_1}{y_0 + L_2} - \tan^{-1} \frac{z_0 + T_2}{y_0 + L_2} + \tan^{-1} \frac{z_0 + T_1 + T_2}{y_0 + L_2} \right] \\ & \left. - 2(y_0 - L_2) \left[\tan^{-1} \frac{z_0}{y_0 - L_2} - \tan^{-1} \frac{z_0 + T_1}{y_0 - L_2} - \tan^{-1} \frac{z_0 + T_2}{y_0 - L_2} + \tan^{-1} \frac{z_0 + T_1 + T_2}{y_0 - L_2} \right] \right\} \end{aligned} \quad (3)$$

Superposition of the forces between four active coils and eight poles of the permanent magnet deduces the total axial force.

$$F_z = l \sum_{i=1}^4 \sum_{j=1}^8 f_{zij} \quad (4)$$

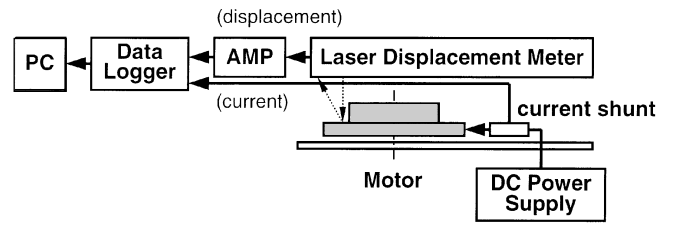


Figure 7. Experimental set-up.

Axial Vibration Response. The axial vibration of the rotor is simplified as the single-degree-of-freedom with respect to the axial displacement z .

$$\ddot{z} + 2\zeta\omega_n\dot{z} + \omega_n^2 z = F_z / m, \quad (5)$$

where $\ddot{z} = d^2z / dt^2$, $\dot{z} = dz / dt$, $2Vw_n = C / m$, $\omega_n^2 = k / m$, t is time, m is a mass of the rotor, C is an axial damping coefficient, and k is a radial stiffness. Because the magnetic force of the motor serves as the axial stiffness, the axial stiffness k consists of not only that of the magnetic bearing k_1 but also that of the motor k_2 . The axial force and the axial stiffness are proportional to the magnetomotive force of the stator coils and, therefore, they are proportional to the motor current. Because the current is determined by operating conditions, i.e., the axial force and the axial stiffness are a function of time, the Runge-Kutta-Gill method was used for numerical calculations.

Experiment

Experimental Procedure. An experimental set-up is shown in Fig. 7. The axial vibration was measured by a laser displacement meter and the motor current was detected through a current shunt resistor. The signals were digitized and sent to a computer where the data was stored.

Results of Experiments. Figure 8 shows the measured transient vibration during startup operation. The characteristics of the vibration were as follows:

At the Beginning of Startup Operation. The rotor and the shaft of the air bearing are in dry contact at the speed lower than a threshold¹⁰ because the thrust magnetic bearing is statically unstable in the radial direction.^{7,8} The restoration force of the air bearing is not induced without rotation, and the radial stiffness of the air bearing is small at the very low speed region. The threshold speed is estimated to be several rotations per second.¹⁰ When the motor current, about 1.0 A, was applied, the rotor started to rotate and was in no contact with the shaft over the threshold speed. The axial lumped repulsive force was applied to the rotor simultaneously and the rotor was displaced $0.18 \times 10^{-3} \mu\text{m}$ to the upper direction. The force F_z was estimated to be 0.20 N using the statically measured datum on the axial stiffness of the thrust magnetic bearing, $k_1 = 1.11 \times 10^3 \text{ N/m}$. ($F_z = 1.11 \times 10^3 \text{ N/m} \times 0.18 \times 10^{-3} \text{ m} = 0.20 \text{ N}$)

During Startup Operation. The axial lumped force induced not only the axial static displacement but also the axial transient vibration. The measured frequency of the vibration was 36.2 Hz, which corresponded to the $1.22 \times 10^3 \text{ N/m}$ axial stiffness. This dynamically

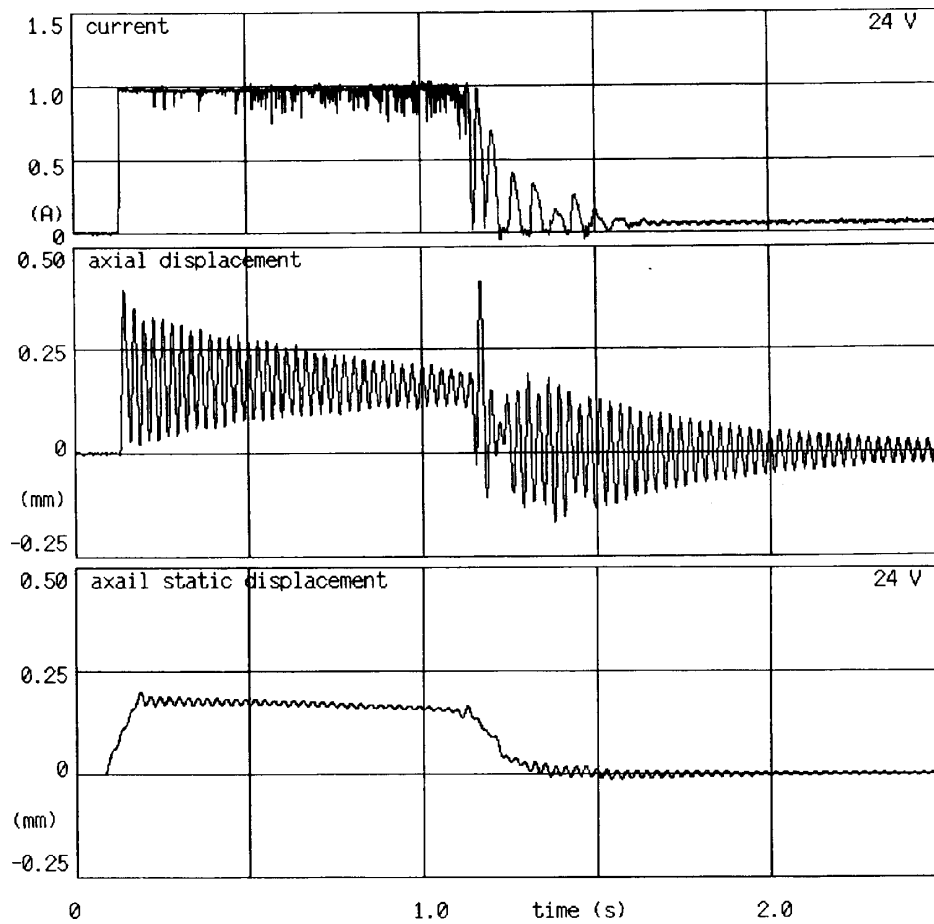


Figure 8. Measured transient vibration during start-up operation. Upper: motor current, Middle: axial displacement of rotor, Lower: axial static displacement derived by averaging the axial vibration for the period of 0.1 second.

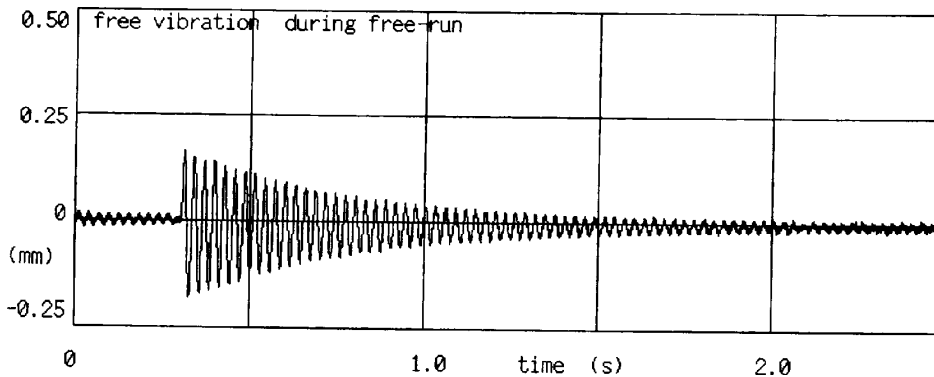


Figure 9. Measured free vibration response during free-run operation. ($\omega_n/2\pi = 34.8$ Hz, $\zeta = 0.01$)

derived stiffness during the startup operation was about 0.12×10^3 N/m higher than the statically measured stiffness at the stationary condition, 1.11×10^3 N/m, and the dynamically measured values during a free-run operation, 1.13×10^3 N/m, and during a rated speed operation, 1.08×10^3 N/m. (The static stiffness was derived dividing weights put on the rotor by the static displacement measured by the laser displacement meter.) The increment corresponded to the stiffness k_2 due to the current passage. The current was almost constant during the startup operation but the occurrence of random pulses of the current decrease was increased in accor-

dance with the increase of the speed. This resulted in the decrease of the averaged current and consequently in the small decrease of the static displacement. The vibration showed viscous-like damping but the damping ratio during the startup operation was a little lower than that during a free-run operation (Fig. 9), because the pulsed current decrease induced a forced vibration. Total startup time was about 1.5 s including a hunting period described below.

Just Before and After Rated Speed. A large hunting of the current was observed just before and after the

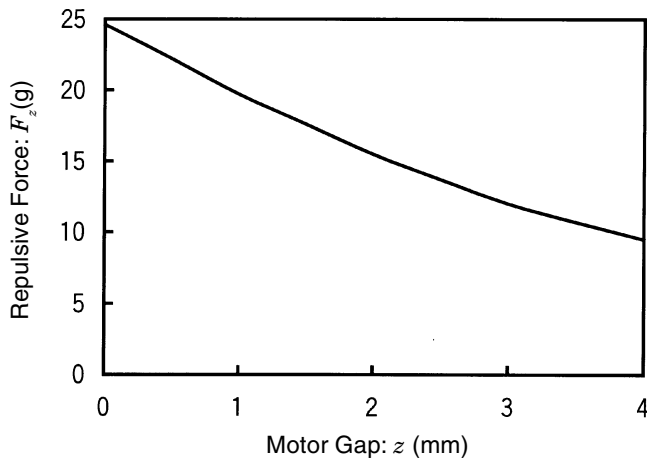


Figure 10. Calculated axial repulsive force of motor at 1.0 A current passage.

rotor speed fell in the rated speed, 15,000 rpm, and this induced the large transient vibration. The hunting period was about 0.5 s. The hunting current must be suppressed by tuning control parameters or, at least, coincidence of the hunting frequency and the natural frequency of the system must be avoided.

During Rated Speed. After the hunting period, the motor current was converged to the rated value, about 0.05 A. The static displacement was also reduced to almost zero. Because the motor current at the constant speed was negligibly small compared with that during the startup operation, the stiffness k_2 was also assumed to be small. Therefore, the stiffness measured during the rated speed, 1.08×10^3 N/m, was almost equal to that of the static value, 1.11×10^3 N/m, and that during the free-run operation, 1.13×10^3 N/m.

TABLE I. Calculated and Measured Force and Stiffness Induced by the Motor at the Rated Gap 0.5×10^{-3} m and 1.0 A Current Passage

	calculated	measured
Repulsive Force F_z	22 g	20 g
Axial Stiffness k_2	7 g/mm	12 g/mm

During Free-Run Operation. Figure 9 shows the axial vibration response during the free-run operation. The response was the free vibration with viscous damping. The measured frequency of the vibration was 34.8 Hz, which corresponded to the 1.13×10^3 N/m axial stiffness and the measured damping ratio was 0.01.

Discussion

Axial Magnetic Force. Axial magnetic force was calculated using Eqs. 3 and 4. Figure 10 shows a calculated relationship between the motor gap and the axial repulsive force induced by the DC motor at 1.0 A operation and Table I summarizes calculated and measured force and stiffness at the rated gap 0.5×10^{-3} m. The force F_z at the rated gap is 0.22 N which coincides with measured value, 0.20 N. The calculated axial stiffness is 0.067×10^3 N/m that is 60% of the measured value, 0.12×10^3 N/m, which includes a cancellation error, because it was derived by the difference of the stiffness under the rated current passage and that without current. Although the model to calculate the magnetic force is preliminary, the calculated result agrees fairly well with the experimental results.

Transient Vibration Response. Figure 11 shows a calculated vibration response. The following parameters are derived from experiments: $mg = 0.231$ N (measured), $C = 0.0001034$ Ns/m (derived from Fig. 9), $k_1 = 1.11 \times 10^3$ N/m (averaged value of the statically measured stiffness at the stationary condition, 1.11×10^3 N/m, and the dynamically measured values dur-

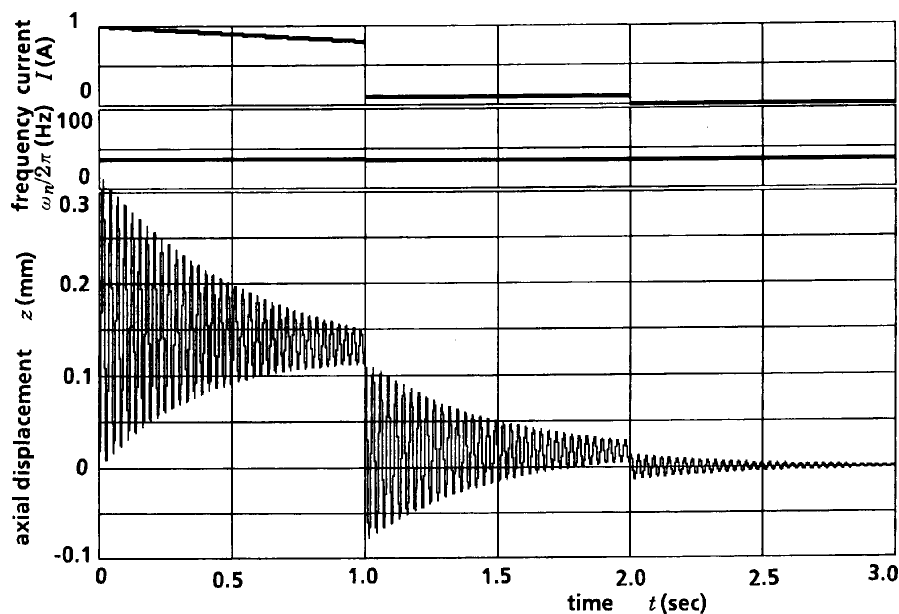


Figure 11. Transient vibration response during start-up operation. (standard)

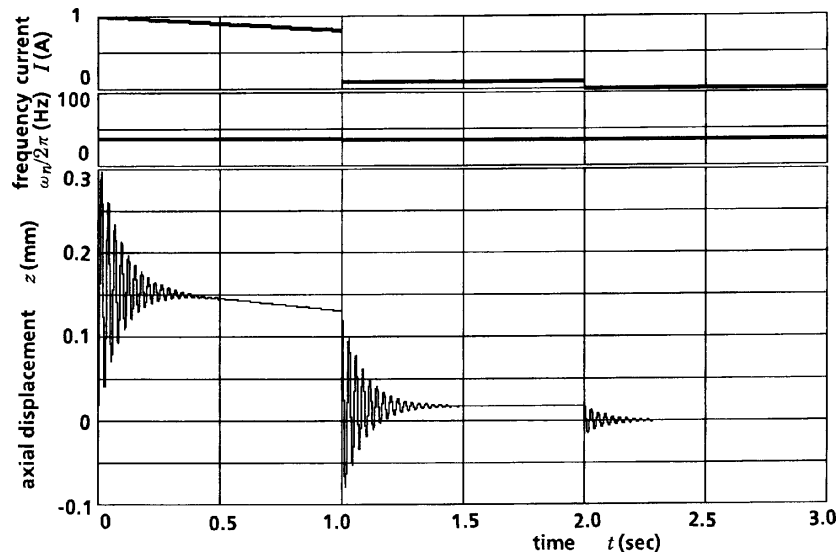


Figure 12. Transient vibration response during start-up operation. (high damping)

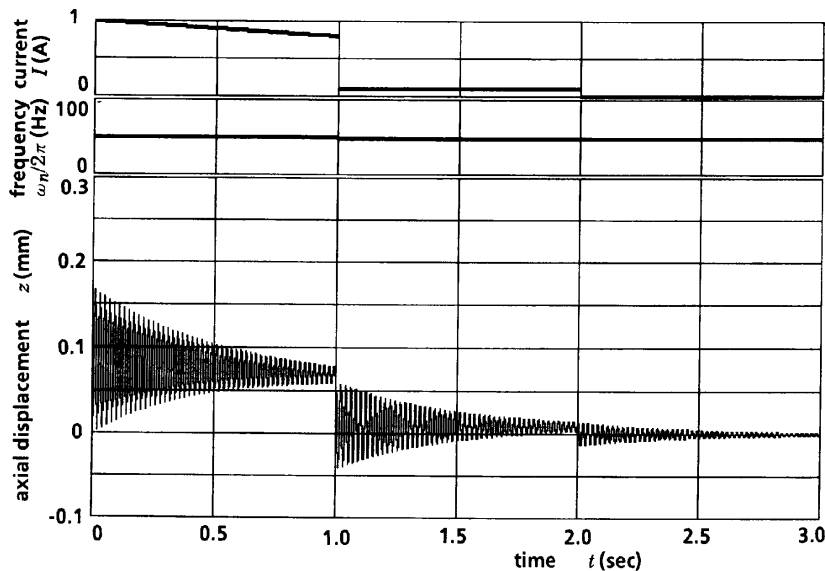


Figure 13. Transient vibration response during start-up operation. (high stiffness)

ing the free-run operation, 1.13×10^3 N/m, and during the rated speed operation, 1.08×10^3 N/m), $k_z / I = 0.118 \times 10^3$ N/(m·A) (based on the theoretical result that the stiffness is proportional to the current), $F_z / I = 0.196$ N/A (based on the theoretical result that the axial magnetic force is also proportional to the current), These values are used not only for the calculation of Fig. 11 but also for the calculations of Figs. 12 through 15 unless otherwise specified.

The calculated response agrees well with the measured shown in Fig. 8 except for the large transient vibration observed just before and after the rotor speed fell in the rated speed. This discrepancy arises because the hunting of the motor current is neglected in the calculation.

Parametric Calculations. Parametric calculations shown in Figs. 12 through 15 deduce the following characteristics on the effect of vibration parameters and operating conditions.

Effect of Damping. Figure 12 shows a calculated response in the case that the damping is five times larger than that of Fig. 11 (standard). It is obvious that the vibration converges faster than the standard case but peaks of the transient vibration are not reduced substantially unless the large damping close to the critical one is applied.

Effect of Stiffness. Figure 13 shows a calculated response in the case that the stiffness of the magnetic bearing is two times larger than that in the standard case. Both the static displacement and the magnitude of the vibration are inversely proportional to the stiffness. However, because the high axial stiffness induces the high radial unstable stiffness,^{7,8} it reduces a lifetime of the air bearing due to the dry contact at the start and stop operation;¹⁰ the stiffness must be determined considering trade-off of the vibration and the lifetime.

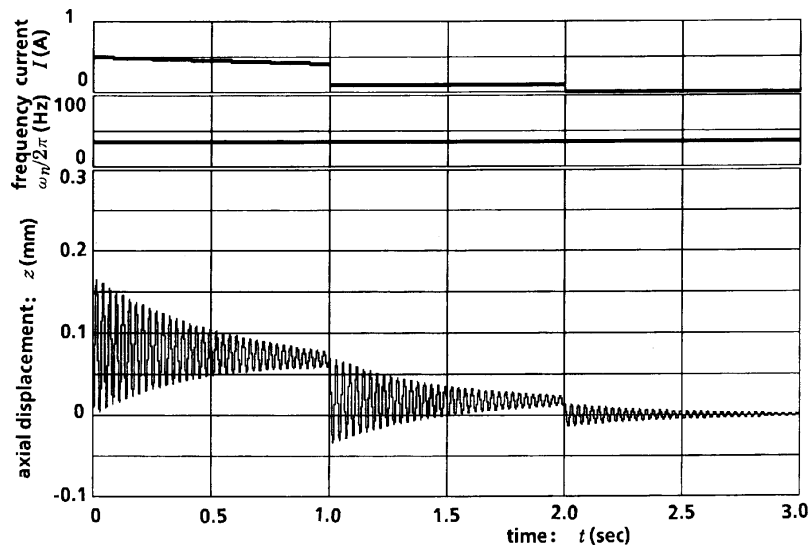


Figure 14. Transient vibration response during start-up operation. (low current)

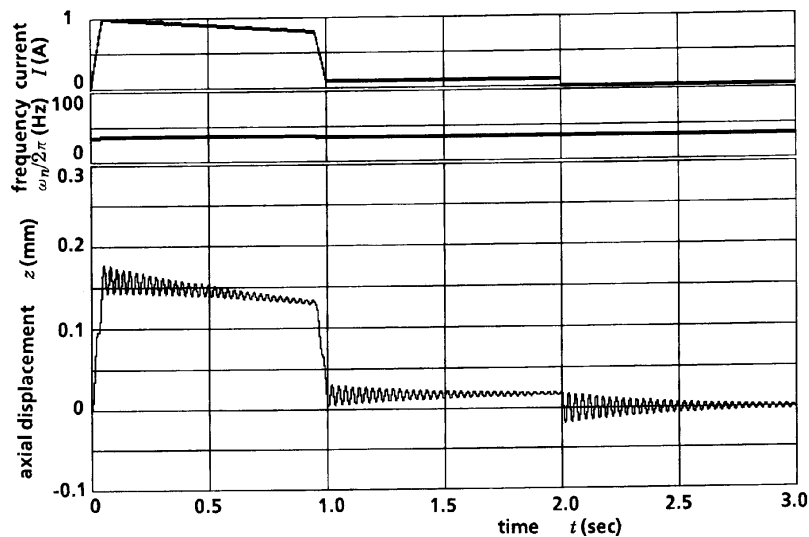


Figure 15. Transient vibration response during start-up operation. (soft start-stop scheme)

Effect of Acceleration Current. Figure 14 shows a calculated response in the case that the current during the start-up operation is one half of that in the standard case. Because the axial repulsive force is proportional to the current, the reduction of the current is also effective to reduce both the static displacement and peaks of the transient vibration if the reduced current is enough to accelerate the rotor speed within an aimed time. On the other hand, because the reduction of the axial stiffness of the motor contributes merely small decrease of the total stiffness, the natural frequency is almost unchanged when the startup current is reduced. The condition of the dry contact at the start and stop operation is not improved even if the startup current is reduced because the radial unstable stiffness of the magnetic bearing is predominant.

Soft Start-Stop Scheme. Figure 15 shows the effect of a soft start-stop operation. The current change at the

start of operation and just before the rated speed is settled, is the soft start-stop scheme. The time of current change is 0.05 s which is negligibly short compared to the total startup time. Drastic effects due to the reduction of the peaks of the transient vibration is achieved by adopting the scheme within the reasonable startup time.

Conclusions

Analytical and experimental investigations have been performed on the axial transient vibration observed at the start-up operation of the polygonal mirror scanner rotor driven by the flat-type brushless DC motor and supported by the passive thrust magnetic bearing and the radial air bearing. From results of investigations, the following characteristics of the vibration and countermeasures to suppress the static displacement and the transient vibration have been deduced.

Mechanism and Characteristics of Vibration. Magnetic force is induced between the stator coils and rotor magnet of the flat-type DC motor under current passage. The total axial force is repulsive and its magnitude is proportional to the current. The force causes the axial static displacement and the axial transient vibration is induced at the start of operation because a large lumped axial force is induced at this moment. The frequency of the vibration is determined by the stiffness of the thrust magnetic bearing and the motor. The stiffness induced by the motor is secondary even at the start-up operation. When the speed falls in the rated speed, the motor current is reduced and therefore the axial repulsive force is reduced. The static displacement is recovered almost to the stationary position because the repulsive force is very small under the constant speed operation. On the contrary, the axial transient vibration is induced again due to the lumped change of the repulsive force. The frequency of the vibration is determined virtually only by the stiffness of the thrust magnetic bearing. A large hunting of the current is sometimes observed just before and after the rotor speed fell in the rated speed and this induced the large transient vibration.

Methods to Reduce Static Displacement and Vibration. Parametric investigation deduced that: (a) higher stiffness of the magnetic bearing and lower acceleration current linearly reduce both the static displacement and the transient vibration; however, the former may reduce the lifetime of the air bearing due to a dry contact with start and stop operation, and the latter prolongs the start-up time; (b) the soft start-stop scheme of the motor current is effective at reducing the vibration.

The hunting current must be suppressed or, at least, coincidence of the hunting frequency and the natural frequency of the system must be avoided. ▲

Acknowledgment. The author would like to express his thanks to Mr. M. Takahashi (Fuji Xerox Co., Ltd.) for his support of this work.

References

1. E. M. Williams, *The Physics and Technology of Xerographic Processes*, Krieger Publishing, Florida, 1993.
2. J. M. Fleischer, M. R. Latta and M. E. Rabedeau, Laser-Optical System of the IBM 3800 Printer, *IBM J. Res. Dev.* **21**, 479 (1977).
3. S. P. Sarraf, Air Spindle for Laser Scanner, *SPIE Vol. 1079*, Hard Copy Output, 443 (1989).
4. J. H. Vohr and C. Y. Chow, Characteristics of Herringbone-Grooved, Gas-Lubricated Journal Bearings, *Trans. Amer. Soc. Mech. Eng. D*, **87**, 568 (1965).
5. K. Ono, A. Iwama, M. Suzuki, T. Iwamura, Y. Itami, and T. Hwang, Analysis and Design of Radial and Thrust Bearing for Polygonal Scanner Rotor-Bearing System, *J. Trans. Japan Soc. Mech. Eng. C*, **60**, 2670 (1996).
6. T. Y. Hwang, K. Ono and Y. Itami, Unbalance and External Excitation Response Characteristics of a Laser Scanner Rotor Supported by Self-Acting Grooved Journal Air Bearings, Proc. of the International Conference on Micromechatronics for Information and Precision Equipment (MIPE'97), IO-07, *The Japan Society of Mechanical Engineers*, JSME Centennial Grand Congress, Tokyo (1997).
7. H. Kawamoto, Stiffness Analysis of Magnetic Bearing—Radial Stable Stiffness of Radial Stable Type Magnetic Bearing, *Bulletin Japan Soc. Mech. Eng.* **216**, 1654 (1983).
8. H. Kawamoto, Magnetic Bearing for High Speed Rotors, Ph.D. Thesis, Tokyo Institute of Technology, 1983.
9. S. Tada, S. Yanabe and Y. Inoue, Axial Vibration of Optical Disk Spindle System, *J. Trans. Japan Soc. Mech. Eng. C*, **62**, 4467 (1996).
10. H. Kawamoto, Rotor Dynamics of Polygonal Mirror Scanner Motor Supported by Air Bearings in Digital Electrophotography, *J. Imaging Sci. Technol.* **41**, 565 (1997).